Development of novel radiolabeled antibody-conjugated graphene quantum dots for targeted in vivo breast cancer imaging and biodistribution studies

Raziyeh Ganji Arjenaki [a], Ghazaleh Samieepour [b], Seyed Esmaeil Sadat Ebrahimi [c], Morteza Pirali Hamedani [c], Mostafa Saffari [d], Mohammad Seyedhamzeh [e], Ali N. Kamali [f], Atena Najdian [a,*], Mehdi Shafiee Ardestani [a,*]

[a] Department of Radiopharmacy, Faculty of Pharmacy, Tehran University of Medical Sciences, Tehran, Iran
[b] Department of Radiopharmacy, International Campus, School of Pharmacy, Tehran University of Medical Sciences, Tehran, Iran
[c] Department of Medicinal Chemistry, Faculty of Pharmacy, Tehran University of Medical Sciences, Tehran, Iran
[d] Department of Pharmaceutics & Medical Nanotechnology, Branch of Pharmaceutical Sciences, Islamic Azad University, Tehran, Iran
[e] Zanjan Pharmaceutical, Nanotechnology Research Center (ZPNRC), Department of Pharmaceutical Nanotechnology, School of Pharmacy, Zanjan University of Medical Sciences, Zanjan, Iran
[f] CinnaGen Medical Biotechnology Research Center, Alborz University of Medical Sciences, Karaj, Iran

ARTICLE INFO

ABSTRACT

Nanotechnology-based drug delivery platforms have emerged as one of the promising approaches for the diagnosis and treatment of cancers. Furthermore, significant advancements have been achieved in the development of nanoparticle-antibody conjugates for applications in tumor imaging and immunoassays. Without a doubt, the diagnostic insight garnered from these nanoprobes will prove invaluable in determining rational therapeutic strategies. In the current experiment, we developed a breast cancer imaging probe utilizing graphene quantum dots, these quantum dots were conjugated with pembrolizumab (GQDs–pembrolizumab), a human monoclonal antibody (mAb) targeting the immune checkpoint programmed death receptor (PD-1) and its programmed death ligand-1 (PD-L1). Various techniques were employed for characterization, encompassing transmission electron microscopy (TEM), element mapping, atomic force microscopy (AFM), Fourier-transform infrared spectroscopy, and circular dichroism (CD) spectroscopy. The toxicity of nanoconjugate was evaluated using the MTT assay on HEK-293 and 4T1 cell lines. Subsequently, the synthesized nanoconjugate was radiolabeled with Technetium-99m (^{99m}Tc) to produce ^{99m}Tc-GQDs–pembrolizumab. Biodistribution and SPECT imaging were conducted to assess the pharmacokinetics and targeting efficacy of the ^{99m}Tc-GQDs–pembrolizumab in a BALB/c mouse model bearing with 4T1 tumors. The high Radiochemical purity (RCP > 95 %) and satisfactory in vitro stability demonstrate the significant potential of GQDs–pembrolizumab to form complexes with Technetium-99m. The findings from imaging and biodistribution studies demonstrated the high activity of ^{99m}Tc-GQDs–pembrolizumab at the tumor site (8.4 %ID/g), attributed to the presence of the PD-1 receptor. Furthermore, the increased radiotracer uptake was evident in the liver and spleen, both being lymphoid tissues. The suitable properties and behavior of ^{99m}Tc-GQDs–pembrolizumab suggest that it holds promise as a novel probe for the development of radiopharmaceutical-based immune checkpoint monoclonal antibodies. Additionally, it has the potential to facilitate immunotherapy for treating a wide range of cancers.

1. Introduction

Among women, breast cancer (BC) stands as one of the most frequently diagnosed cancer globally. In the year 2023, it is projected that there will be nearly 300,590 new cases of BC in the United States, which translates to approximately 825 cases each day. Moreover, the

projected number of BC-related deaths is anticipated to reach 43,700 (Siegel et al., 2023). By the year 2040, it is predicted that the rate of newly diagnosed cases of BC and the rate of deaths resulting from BC will experience an increase of over 40 % and 50 %, respectively, compared to the statistical data of 2020 (Arnold et al., 2022). Hence, the significance of improving imaging modalities or combining two (or more) imaging techniques (e.g., single-photon emission computed tomography/computed tomography (SPECT/CT) and positron emission tomography/computed tomography (PET/CT)) increases the evaluation and early detection of BC (Simanek and Koranda, 2016).

Immunotherapy, as a promising therapeutic strategy, has experienced substantial advancements over the past decade (Ehlerding et al., 2016, Passiglia et al., 2016, Marhelava et al., 2019). Novel therapeutics that target immune checkpoints have the potential to landscape of cancer therapy, resulting in sustained responses for conditions such as non-small cell lung cancer, melanoma, breast cancer, renal cell cancer, and gastric cancer (Wang et al., 2017, Lee et al., 2017, Lee et al., 2016, Hsueh and Gorantla, 2015, Brahmer et al., 2015). A pivotal focus of immunotherapy is centered on the axis involving the immune checkpoint programmed death receptor (PD-1) and its programmed death ligand-1 (PD-L1). This axis serves to regulate autoimmunity within healthy tissues and evade detection by the immune system. However, this factor facilitates an immune escape mechanism for malignant cells within the tumor microenvironment (Boussiotis, 2016). PD-1 is a cell surface protein that plays a pivotal role in the suppression of the immune response by actively inhibiting T cells. PD-1 has two ligands, primarily PD-L1, the most widely expresses ligand, and PD-L2. PD-L1 is mainly expressed on tumor cells and immune cells but PD-1 is expressed on activated T-cells, B-cells, and macrophages (Hamid and Carvajal, 2013). The Food and Drug Administration (FDA) has approved antibodies-based inhibitors of PD-1/PD-L1, which include Pembrolizumab (Merck), Nivolumab (Bristol-Myers Squibb), Atezolizumab (Roche), and Durvalumab (AstraZeneca), for numerous types of malignancies (Saresella et al., 2012; Carbognin et al., 2015). Pembrolizumab is a fully humanized IgG$_4$ kappa monoclonal antibody that effectively obstructs the PD-1 receptor, resulting in anti-tumor activity (Inokuchi and Eto, 2019, Kwok et al., 2016). Recent investigations involving ^{89}Zr and ^{64}Cu-radiolabeled pembrolizumab have indicated the specific targeting of PD-1 receptor in mice and rats. These studies revealed a substantial accumulation of radiotracer in the liver and spleen (England et al., 2017, Natarajan et al., 2018). In this context, Van der Veen et al. examined the in vivo biodistribution of ^{89}Zr-pembrolizumab using both humanized (huNOG) and non-humanized NOG mice that were engrafted with human A375M melanoma cells. PET imaging and the findings from biodistribution studies exhibited substantial radiopharmaceutical accumulation in both the lymphoid system and tumor cells. These results validate the presence of PD-1 and suggest a comprehensive assessment of the radiotracer's whole-body biodistribution in cancer patients with cancers before initiating treatment with PD-1 antibodies (van der Veen et al., 2020). Immune-SPECT/PET imaging not only assessed the disease progression and treatment response in various cancer types but also circumvented the need for initial and repetitive biopsies (Broos et al., 2018).

The potential application of nanoparticles as carriers for delivering therapeutic and diagnostic agents has generated substantial interest (Mura et al., 2013, Xu et al., 2016, Najdian et al., 2022, Chinen et al., 2015, Ghoreishi et al., 2020). Molecular imaging agents constructed from targeted functional nanoparticles enable the visualization of distinct tissues and pathological lesions by enhancing the signal-to-noise ratio. Consequently, they have the potential to enhance cancer diagnostics and treatment management (Lee et al., 2012, Cassette et al., 2013). Graphene quantum dots (GQDs), an emerging luminescent carbon-based nanomaterial, have garnered increasing attention in recent years due to their numerous exceptional physical and chemical properties. The two-dimensional hexagonal lattice structure of these nano-sized single sheets of graphene fragments results in the

manifestation of quantum confinement (Pan et al., 2010, Li et al., 2013, Zhou et al., 2012). Several superior properties of GQDs are including: i) strong chemical inertness; ii) luminescence emission, iii) photostability, iv) excellent biocompatibility, v) tunable low cytotoxicity, vi) high solubility, vii) photothermal properties, and viii) high surface area (Zheng et al., 2015, Kumar et al., 2020). In 2019, Wang et al. published a report detailing the synthesis and utilization of functionalized and radiolabeled GQDs for in vivo imaging of mice with tumor-bearing conditions (Wang and Wei, 2019). The SPECT images and biodistribution study data of iodine-131 (^{131}I)-labeled polyethylene glycol and folic acid co-functionalized GQDs revealed substantial accumulation at the tumor site, with the renal system identified as the primary route of excretion. However, the liver played a significant role in the clearance of the radiotracer. Moreover, nanosized GQDs doped with both nitrogen and boron (5 nm) were prepared for near-infrared (NIR II) fluorescence imaging and photothermal therapy in nude mice. These GQDs exhibited favorable characteristics, including prolonged blood-circulation half-life, minimal toxicity and rapid excretion (Wang et al., 2019).

Radionuclides employed in the SPECT modality emit gamma rays within the energy range of approximately 75 to 360 keV. Until now, in the field of diagnostic nuclear medicine, Technetium-99m (^{99m}Tc) stands as the most widely utilized radionuclide due to its optimal physical properties (T $_{1/2}$= 6 h, E$_\gamma$ = 140 keV). This radionuclide allows for effective SPECT imaging while also ensuring patient safety (Psimadas et al., 2013, Banerjee et al., 2001). In addition, ^{99m}Tc offers advantageous attributes such as widespread availability, favorable coordination chemistry, and rapid and convenient labeling of various chemical compounds (Liu and Edwards, 1999).

Nanoparticles-antibody conjugates have emerged as promising system that enhance sensitivity and precision in in vitro diagnostics such as immunoassays. Meanwhile, in vivo applications have harnessed the targeting capability of nanoparticle-antibody conjugates, as well as their adaptable payload and customized biodistribution. In other words, nanoparticle-antibody conjugates have been depicted as a feasible method to enhance targeting capability of nanoparticles and their retention within the desired tissue (Lin et al., 2021). In this regard, antibody-conjugated gold nanoparticles (GNPs) have been employed to improve the quality of imaging and offer anatomical insights into preclinical tumor tissues. Both enhanced signal attenuation and improved tissue retention are the result of in vivo functionality and tissue specificity of GNPs and their conjugates with antibodies, enhancing them to outperform typical CT contrast agents (Popovtzer et al., 2008, Lijowski et al., 2009). For an example, Kao et al. conducted a study in which they developed ^{111}In-PEGylated GNPs conjugated with Cetuximab-an antibody targeting the epidermal growth factor receptor (Kao et al., 2014). This study demonstrated high uptake in A549 cells, a cell line with high EGFR expression. This uptake was significantly augmented, exhibiting an average increase of 14.8-fold when compared to non-conjugated GNPs. Furthermore, this study emphasizes the role of nanoparticle-antibody conjugates in facilitating interactions between NPs and cell, promoting the internalization of NPs by host cells. This process contributes to enhanced imaging contrast through increased retention of NPs within tissues. Moreover, dendrimers encapsulated gold nanoparticles, incorporated gadolinium, and conjugated to an anti-human HER-2 antibody were developed for magnetic resonance imaging (MRI) and computed tomography (CT). This dual-modal imaging agent demonstrated a significant increase in MRI signal intensity by approximately 20 % and a two-fold improvement in CT resolution and contrast after intravenous administration in mice with HER-2-positive tumors. Flow cytometry and confocal microscopy analyses provide validation of the specific targeting and internalization of this nanoparticle-antibody conjugate in human HER-2 positive cells (Chen et al., 2020).

In this paper, we formulated a biocompatible nanoparticle-antibody conjugate radiolabeled with ^{99m}Tc, serving as a SPECT imaging nanoprobe. This radiolabeled nanoconjugate, incorporating GQDs and

pembrolizumab, was designed for targeted imaging of breast cancer. Biodistribution studies and SPECT scans were carried out on both normal and 4T1 tumor-bearing BALB/c mice, offering valuable insight into the in vivo behavior and potential of the developed radiotracer for targeted imaging.

2. Experimental

2.1. Materials and methods

In this experiment, citric acid and urea were purchased from Merck (Darmstadt, Germany). Other chemical reagents and solvents utilized in the study were purchased from Sigma Aldrich (MO, U.S.A.) in analytical grade and were employed without the need for additional purification. The human embryonic kidney 293 (HEK-293) cells and mice breast adenocarcinoma (4T1) cell lines were purchased from the Pastor Institute (Tehran, Islamic Republic of Iran). N-terminal α-amino group modification of pembrolizumab was gifted from CinnaGen company (Alborz, Islamic Republic of Iran).

For characterization, element mapping, transmission electron microscopy (TEM), and scanning electron microscopy (SEM) was conducted using TESCAN and ZEISS instruments. Atomic Force Microscopy (AFM, CP-RESEARCH model, VEECO, USA) was also performed. An infrared spectrum was obtained on a Perkin Elmer Spectrum BX-II spectrometer. The determination of antibody conformation and the investigation of pembrolizumab's interaction with GQDs were conducted using circular dichroism (CD) spectroscopy. CD experiments were performed using Aviv CD spectrometer within a wavelength range of 190 and 250 nm. A quartz cell with a path length of 0.1 cm was employed for these measurements. Sodium pertechnetate ($Na^{99m}TcO_4$) was readily generated from a commercial Molybdenum 99/Technetium-99m ($^{99}Mo/^{99m}Tc$) generator (Radioisotope Division, AEOI) using isotonic sodium chloride solution (pH = 7.4). SPECT imaging was carried out using a Dual-head γ- camera (E.cam, Siemens, Germany). Moreover, quantitative gamma counting was performed on an ORTEC Model 4001 M c-system well counter. For biodistribution studies, female BALB/c mice weighing 23–27 g and aged six to seven weeks were utilized. These mice had been injected subcutaneously with 4T1 cells in the right flanks. Throughout the study, they were provided with unrestricted access to water and standard laboratory food. All studied experiments conducted in this study were repeated three times. Animal research was conducted in accordance with the approved guidelines of the Animal Care and Use Committee of Tehran University of Medical Sciences (#IR. TUMS. MEDICINE.REC.1401.108).

2.2. Synthesis of GQDs

In this research, GQDs were synthesized using a one-pot hydrothermal method, employing citric acid and urea as the precursor materials. In brief, citric acid (1 mmol) and urea (3 mmol) were dissolved in 5 mL of deionized water. Subsequently, the solution was transferred into an autoclave and subjected to heating at 160 °C for a duration of 4 h. The resulting product was allowed to cool down to room temperature. To eliminate impurities, centrifugation was carried out by adding ethanol, followed by a dialysis process using dialysis membrane with a molecular weight cut-off of 1000.

2.3. Conjugation of synthesized GQDs to pembrolizumab

First, 20 mg of GQDs were dissolved in a mixture of DMF and water (4 mL). Subsequently, 0.02 mmol of EDC and 0.01 mmol of NHS were introduced into the solution while stirring for a duration of 30 min at room temperature. In the next step, the pH of the reaction mixture was adjusted to 9. Afterward, 2 mg of pembrolizumab was added to the solution and allowed to reacted for 7 h while stirring at room temperature. The resulting nanoconjugate was purified to remove residual EDC and

NHS, and unconjugated pembrolizumab. This was achieved by washing the solution with 25 mM HEPES buffer and utilizing centrifugation at 20,000 rpm for 15 min.

2.4. Calculation of chelator-antibody ratio (CAR)

For the CAR calculation, deferoxamine preparation for the standard curve were adjusted to various concentrations (198–26 μM in 0.25 M NaOAc pH5.5), and the blank control sample was adjusted to 9 mg/mL (60 μM). A total of 225 μL of sample or standard was added to 96 wells in a plate, followed by addition of 25 μL of 50 mM Fe (II) to each well. After the plate was shaken at 700 rpm for 1 h at room temperature, the absorbance at 450 nm was measured and the concentration of DFO in sample was calculated (Kono et al., 2021).

2.5. MTT assay

Cell viability was assessed using the 3-(4,5-dimethylthiazol-2-yl)-2,5-diphenyl-tetrazolium bromide (MTT) assay. This procedure was conducted on both the HEK-293 and 4T1 cell lines, following the methods outlined in previously published articles (Rai et al., 2018, van Meerloo et al., 2011, Nikzad et al., 2013). In brief, cells were seeded into 96-well plates at a density of 5000 cells per well and then incubated in a CO_2 incubator at 37 °C for 24 h. Subsequently, the cells were treated with varying concentrations of the nanoconjugate (ranging from 5 to 500 μg/mL) for 48 h. Afterward, 50 μL of the prepared MTT solution (5 mg/mL in phosphate buffered saline) was added to each well treated with nanoconjugate, followed by incubation at 37 °C and 5 % CO_2 for 3 h. Subsequently, 150 μL dimethyl sulfoxide (DMSO) was used to dissolve purple formazan crystals. Then, the absorbance of each well was measured at a wavelength of OD = 570 nm. The resulting data were then compared to the absorbance obtained from the control group, which consisted of untreated cell cultures.

2.6. ^{99m}Tc radiolabeling of GQDs–pembrolizumab conjugate

In a typical procedure, a lyophilized kit containing the GQDs–pembrolizumab conjugate was prepared. Initially, 20 mg of nanoconjugate was dissolved in 2 mL of distilled water. Afterward, 0.2 mL of a tin chloride solution (5 mg/1 mL) was added as a reducing agent, along with 0.5 mL of ascorbic acid (5 mg/ 1 mL) as an antioxidant agent. During this step, the pH of the solution was adjusted to 7.4 using sodium hydroxide solution. The resulting solution was then subjected to lyophilization. For the radiolabeling process, the prepared kit was incubated with 200 μL of $Na^{99m}TcO_4$ (370 MBq) that had been freshly eluted from the $^{99}Mo/^{99m}Tc$ generator. This incubation was carried out for a duration of 25 min within an ultrasonic bath.

2.7. Radiochemical purity

To assess the radiochemical purities (RCPs) and ensure accurate radiolabeling of the ^{99m}Tc-nanoconjugate, thin-layer chromatography (TLC), a swift and straightforward method, was employed (Amin et al., 1997, Decristoforo et al., 2007). This was carried out as follows:

A piece of Whatman paper was used as the stationary phase, while methanol/acetone (1:1) and saline were utilized as the mobile phases. For the experiment, 5 μL of the radiolabeled samples were placed at the origin of two paper strips measuring 1.2 × 10 cm. These spots were allowed to dry before initiating the solvent development process. Subsequently, the strips were placed in the scintillation vials. Following the migration of solvent, the developed strips were divided into 10 equal segments and subjected to activity counting using a γ well-type counter. When saline was used as the mobile phase, both $^{99m}TcO_4$ and ^{99m}Tc-GQDs–pembrolizumab migrated on the TLC, while $^{99m}TcO_2$ ($R_f = 0$) remained at the origin. Consequently, the percentage of $^{99m}TcO_2$ was determined using this route. On the other hand, when an ethanol/
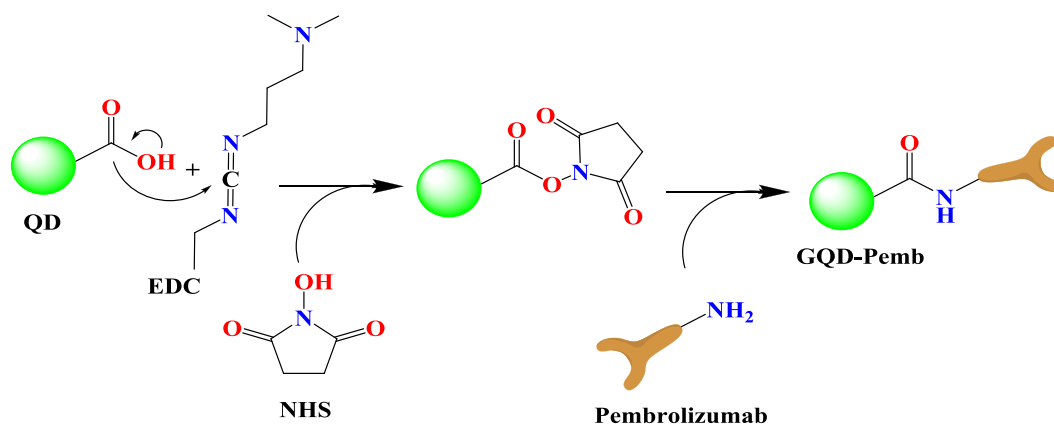
Scheme 1. Mechanism of GQDs conjugation with pembrolizumab antibody.

acetone (1:1) mixture was employed as the mobile phase, only $^{99m}TcO_4^-$ migrated, and both ^{99m}Tc-GQDs–pembrolizumab and $^{99m}TcO_2$ remained at the origin ($R_f = 0$). Therefore, the percentage of free pertechnetate was calculated. Ultimately, the RCP was determined using the following formula:

$$RCP = 100 - (\text{free pertechnetate} + {}^{99m}TcO_2)$$

Moreover, the radiolabeling efficiency or RCP of ^{99m}Tc-GQDs–pembrolizumab was assessed using a standard Radio-TLC with saline as the mobile phase. The radioactivity at various points of the TLC paper was evaluated using a radio-TLC scanner (AR-2000 radio-TLC Imaging Scanner). Any byproducts resulting from the radiochemical reaction and any free ^{99m}Tc, if present, were isolated using an ultrafiltration tube with a cutoff 10 kDa. The precipitate was then resuspended in 500 μL of saline.

2.8. In vitro stability evaluation

The labeling efficiency of the radiotracer was investigated at various time intervals (6, 12, 24, and 48 h) through an in vitro stability test. In this process, 400 μL of ^{99m}Tc-GQDs–pembrolizumab (20 MBq) was incubated in 1000 μL of human serum at 37 °C and in another 1000 μL of PBS at 4 °C. Following this, 100 μL of 10 % trichloroacetic acid was added to the mixture at specific time points. Subsequently, the serum proteins were separated through centrifugation at 4000 rpm at 37 °C for a duration of 4 min. The RCP of ^{99m}Tc-GQDs–pembrolizumab in the plasma was measured using chromatography.

2.9. Scintigraphy

The radiolabeled ^{99m}Tc-GQDs–pembrolizumab underwent in vivo whole-body scintigraphy studies. In this regard, female BALB/c mice (6–7 weeks old, weighing 23–27 g, n = 3) were utilized. These mice were injected subcutaneously in the right flanks with 4T1 cells (1×10^4). All the mice were anesthetized through an intraperitoneal injection of ketamine-xylazine solution. Afterward, 7.4 MBq of ^{99m}Tc-GQDs–pembrolizumab was injected into the mice through the tail vein. The anesthetized mice were then placed in a horizontal position under the SPECT/CT imaging system. Approximately, one hour after the radiotracer injection, images were acquired using a matrix size of 256×256 and an energy window set at 20 % with 140 keV.

2.10. Biodistribution studies

The biodistribution and excretory pathway of ^{99m}Tc-GQDs–pembrolizumab were investigated in BALB/c mice bearing 4T1 tumors (weighing 23–27 g; n = 3). To this end, the mice were anesthetized prior to the radiotracer administration. Subsequently, 150 μL of ^{99m}Tc-

GQDs–pembrolizumab (3.7 MBq) was intravenously injected via the tail vein. The mice were sacrificed 120 min after the radiotracer injection, and the organs of interest were extracted and washed with isotonic sodium chloride solution. The activity counts of each respective organ were then determined using a calibrated gamma counter. The collected data were ultimately presented as a percentage of the administered activity per gram of tissue.

2.11. Statistical analysis

Statistical analysis in this study was performed using Box–Behnken and MATLAB software. A significance level of $P < 0.05$ was deemed statistically significant. Graphs were generated using GraphPad Prism software, version 9.

3. Results

3.1. Structural characterization of GQDs and GQDs–pembrolizumab conjugate

The synthesis of GQDs and the conjugation procedure have been previously elaborated. A schematic representation of GQDs conjugated to pembrolizumab is depicted in Scheme 1. For the purpose of identifying nanoparticle structure and comprehending their morphology, size, and shape, TEM with high-resolution (better than 0.1 nm) could be applied. Therefore, TEM is recognized a prevalent method for characterizing of GQDs (Jia et al., 2011, Guo et al., 2020). Fig. 1 presents TEM image and the size distribution of the synthesized GQDs. The quasi-spherical shape of these nanoparticles displays a planar structure with an average diameter of 4.22 ± 1.5 nm. Following the conjugation of pembrolizumab with GQDs, the size and surface morphology of the resulting nanoconjugate were investigated using the AFM method. As shown in Fig. 2, both two-dimensional (2D) and 3D images of GQDs–pembrolizumab are provided. Based on the data analysis, the GQDs–pembrolizumab nanoconjugates exhibited an average diameter within the range of 21–25 nm. In addition, the energy dispersive spectroscopy (EDS) map (depicted in Fig. 3) represented that the composition of the interior of the nanoconjugates predominantly comprised carbon (C), oxygen (O), nitrogen (N), and sulfur (S) elements. FTIR spectroscopy is a valuable technique that can provide important insights into the functional groups participating in the interaction between nanoparticles and proteins (Mahmoudi et al., 2011). Fig. 4 displays the FTIR spectrum of GQDs showing peaks at 3420 cm^{-1}, 3240 cm^{-1}, and 1722 cm^{-1}, which were attributed to the stretching vibrations of —OH, —NH, and C=N or C=O (the protonation state of the carboxylic group (COOH)) functional groups, respectively. Symmetric stretching mode of COO$^-$ indicated a peak at 1405 cm^{-1}. A peak observed in the 1150–1300 cm^{-1} can be assigned to C—O stretch of —COOH, indicating the
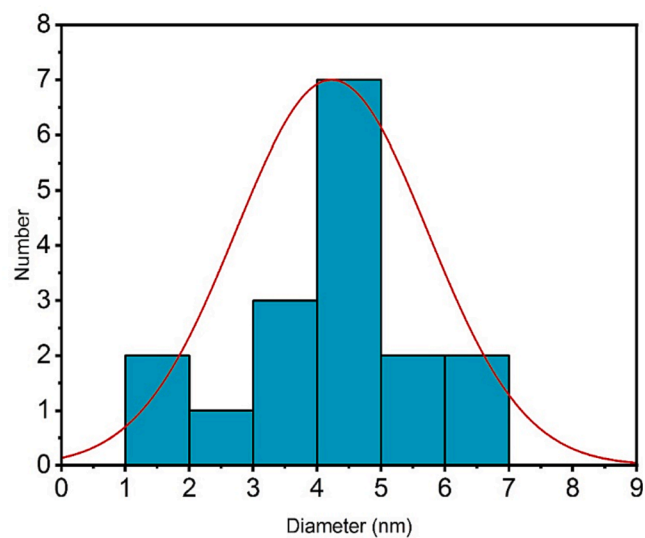
A)
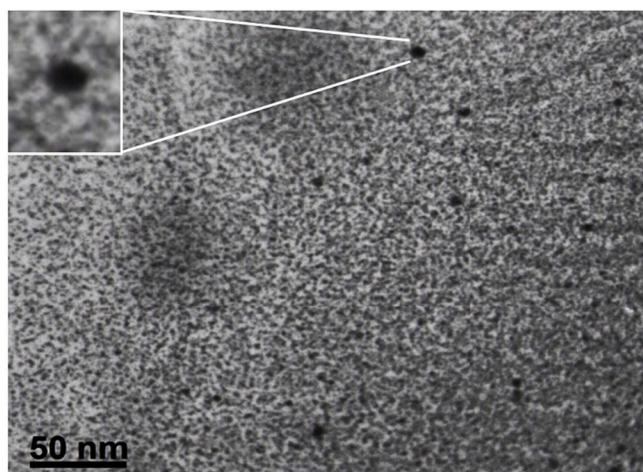
B)

Fig. 1. A) TEM image of GQDs (scale bar: 50 nm). B) Size distribution of the particles with an average diameter of approximately 4.22 ± 1.5 nm.
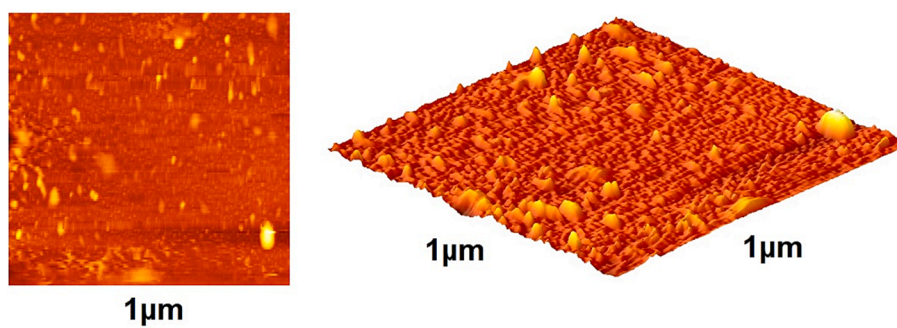

Fig. 2. Atomic force microscopic analysis of GQDs–pembrolizumab conjugate (2D (Left) and 3D (Right) images).
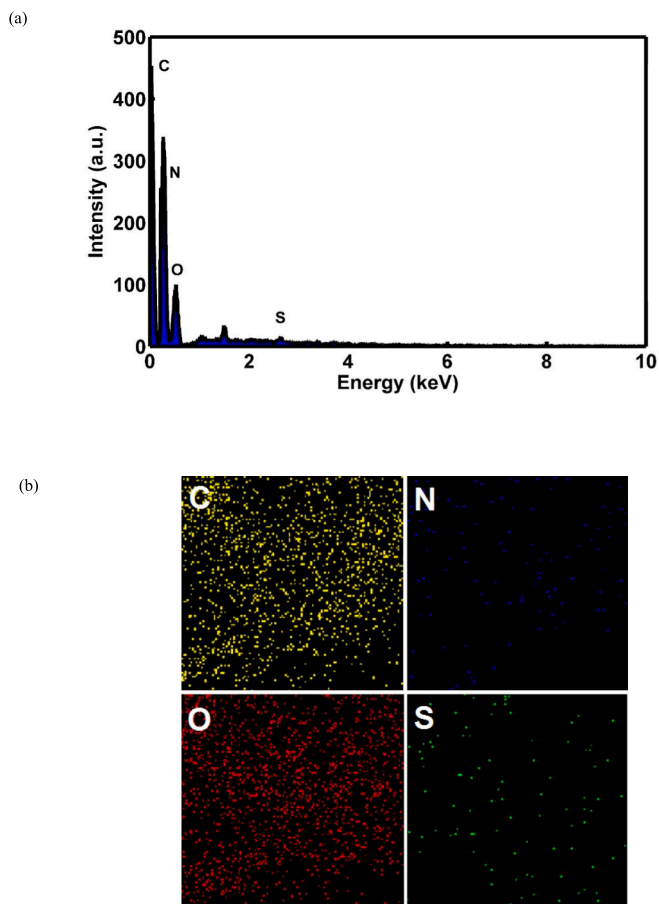
(a)

(b)

Fig. 3. EDS-mapping pictures of GQDs–pembrolizumab. (a) EDS diffraction pattern of nanoconjugate, (b) abundance image of C element, abundance image of N element, abundance image of O element, and abundance image of S element.

presence of hydroxyl and carboxyl functional groups on the surface of GQDs (Gu et al., 2020). Notably, the peak corresponding to the C═O stretching vibration adsorption in the nanoconjugate's spectrum was
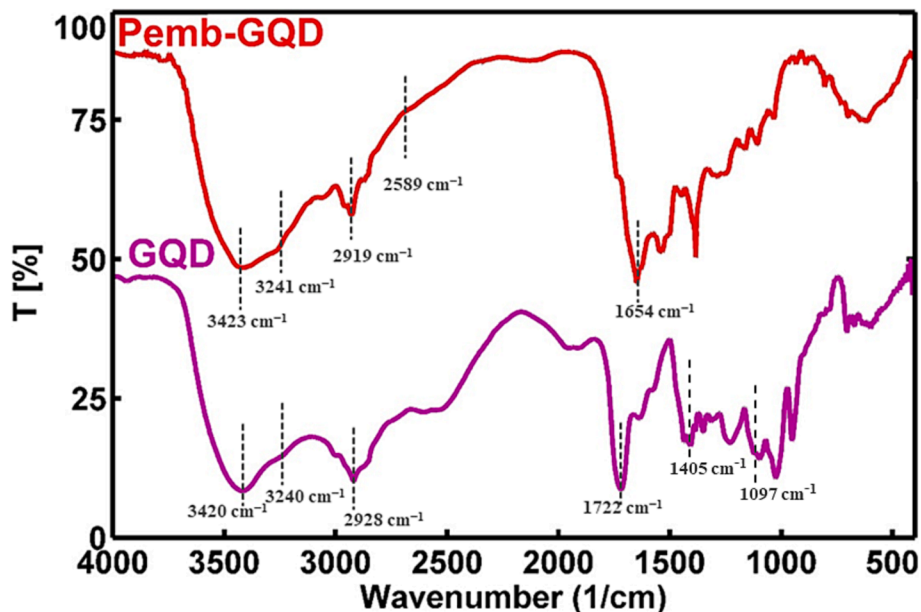
observed at a lower wavenumber, indicating successful conjugation. Additionally, the presence of amide bonding was confirmed by the peak at 1654 cm^{-1}. Moreover, a characteristic peak at 2928 cm^{-1} signifies C—H stretching vibrations. A faint peak at 2589 cm^{-1} indicates the presence of thiol groups within the structure. The analysis of FTIR spectra revealed the presence of surface oxygen and nitrogen functional groups in the products, attached to edge or basal plane of GQDs. In addition, the obtained results were comparable to those of the previously synthesized GQDs (Hassanpouraghdam et al., 2022, Ryu et al., 2014). An essential issue consideration during the conjugation of nanoparticles with proteins is ensuring the preservation of the protein's structure and function. The study employed CD spectroscopy to assess the secondary structure of pembrolizumab within the GQDs–pembrolizumab conjugate. Fig. 5 presents the spectra of free pembrolizumab (depicted by the blue line) and GQDs–pembrolizumab (illustrated by the green line). The results showed minimal alteration in the structure of pembrolizumab. Both CD spectra exhibited negative absorbance around 220 nm, indicative of a β-sheet-rich structure. Importantly, the secondary structure of pembrolizumab remained unchanged even after
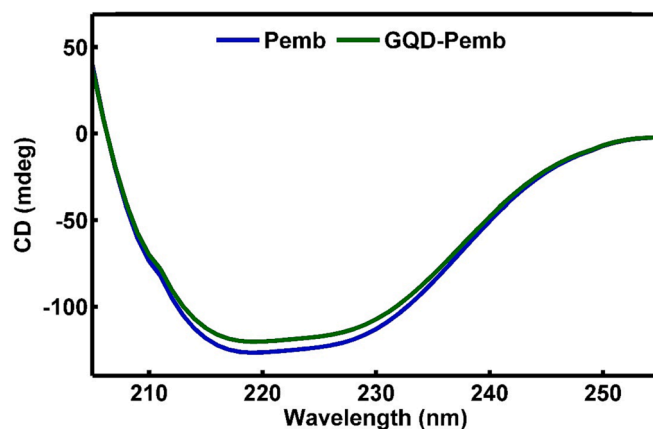

Fig. 5. Far ultraviolet region circular dichroism spectra of free antibody (blue), GQDs–pembrolizumab conjugates (green). (For interpretation of the references to color in this figure legend, the reader is referred to the web version of this article.)
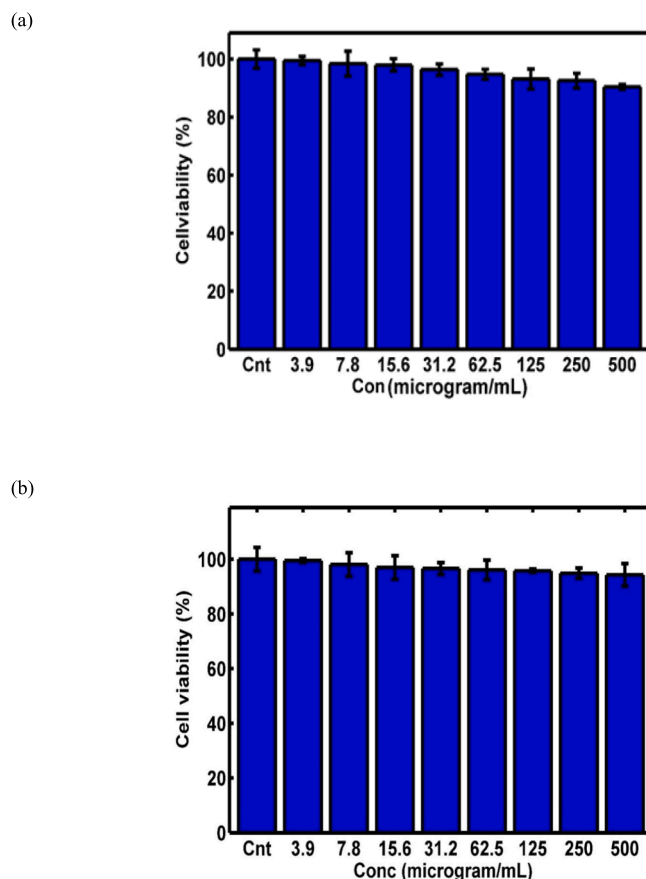

Fig. 4. FTIR spectra of GQDs and GQDs–pembrolizumab.

(a)

(b)

Fig. 6. MTT assay results for GQDs–pembrolizumab conjugates (a) and pembrolizumab (b) on the HEK-293 cell line, as well as the MTT assay results for GQDs–pembrolizumab conjugates (c) and pembrolizumab (d) on the 4 T1 cell line, with a significance level indicated by "P value < 0.05".

conjugation with GQDs, a critical aspect for the application of these materials in biomedicine.

3.2. MTT assay

The MTT assay was conducted on both the HEK-293 and 4T1 cell lines to evaluate the cytotoxicity of pembrolizumab and GQDs–pembrolizumab conjugates. The concentrations studied for the HEK-293 cell line were 0, 3.9, 7.8, 15.6, 31.2, 62.5, 125, 250, and 500 µg/mL for. For the 4T1 cell line, the concentrations studied were 1.25, 2.5, 5, 10, 15, 25, 50, 75, and 100 µg/mL. The resulting viability values plotted against concentrations are depicted in Fig. 6. Upon exposure of the HEK-293 cell line to the specified concentrations of pembrolizumab and the nano-conjugate, up to 500 µg/mL for 48 h, no significant toxicity was observed compared to the control group. However, treatment of the 4T1 cells with higher concentrations of pembrolizumab and the nano-conjugate after 48 h led to considerable reduction in cell viability, attributed to the heightened sensitivity of these cells. The MTT assay was conducted in triplicated.

### 3.3. Radiolabeling and quality control of ^{99m}Tc-GQDs–pembrolizumab

The radiolabeling protocol was developed by our research team (Ghoreishi et al., 2020). In brief, various parameters affecting the labeling process were taken into consideration, including the quantity of reducing agent, amount of GQDs–pembrolizumab, and the reaction time. Details of these parameters are provided in Tables 1 and 2. The Box–Behnken software was then employed for statistical analysis, and the results of variance analysis are presented in Table 3 (P value < 0.05).

Plus and minus signs indicated the potential direct and indirect effects of the studied parameters, respectively. The results of two-term interactions on the average mean of the third term are illustrated in Fig. 7. Changes in the intensity of the green color reflected variations in the response. The optimal levels of the studied variables were determined and are documented in Table 4. Ultimately, the ideal conditions for achieving a high radiolabeling yield were found to be 5 mg of reducing agent, 20 mg of nanoconjugate, and an incubation time of 25 min. Ensuring the preparation of a lyophilized kit prior to radiolabeling was crucial in order to minimize the impact of oxygen on the technetium-99 m solution. This step helped maintain the stability and reliability of the radiolabeling process. To determine the RCP using TLC, the activities of the labeled samples on the strips were measured using a γ well-type counter. This analytical technique allowed for the separation and identification of different components in a mixture based on their migration rates of a thin layer of adsorbent materials. The γ well-type counter was used to measure the radioactivity of the separated components, providing valuable information about the success of the radiolabeling process and the purity of the final product. Moreover, the radiolabeling efficiency the ^{99m}Tc-GQDs–pembrolizumab was evaluated using radio thin-layer chromatography (radio-TLC), as shown in Fig. 8a.

3.4. Stability studies

In the conducted in vitro stability tests, (Najdian et al., 2022) the radiotracer was exposed to two different conditions: PBS at 4 °C and human serum at 37 °C, both over a 48-hour period. The results, as shown in Fig. 8b, indicated that there was minimal transchelation (about 4–5 %) in PBS and less than 20 % in human serum. This demonstrated that
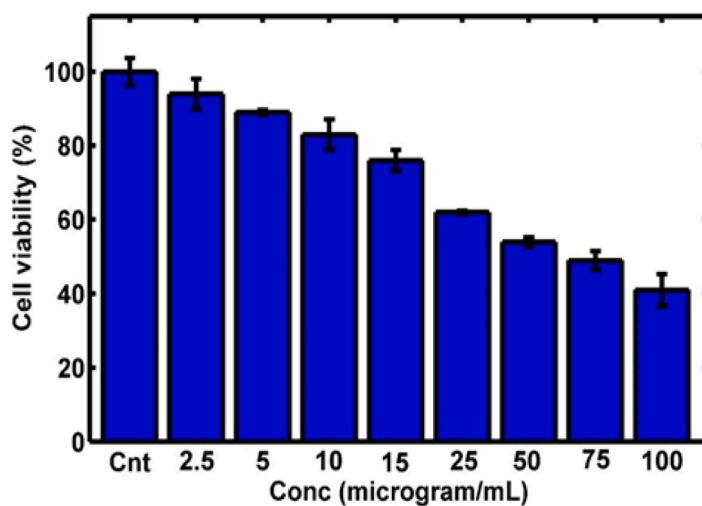
(c)
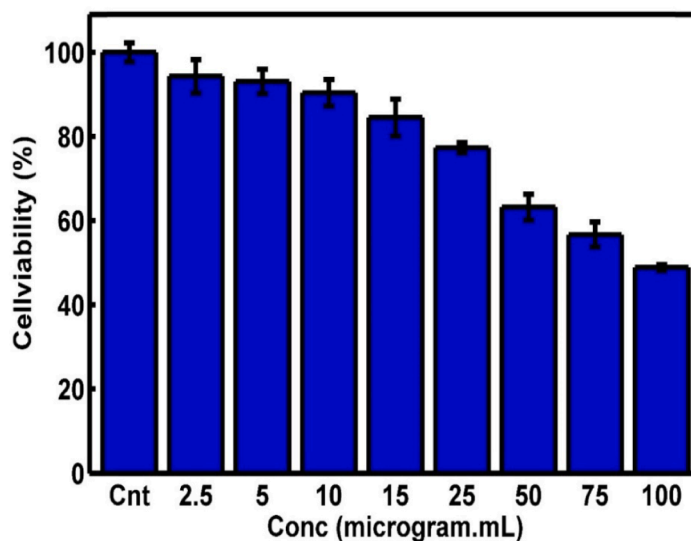
(d)

Fig. 6. (*continued*).

Table 1
The effective Parameters on radiolabeling yield.

Factor	Units	−1	0	1
Reduced Agent	mg	3	5	7
GQDs–pembrolizumab	mg	10	15	20
Time	min	15	20	25

Table 2
Data of radiolabeling design.

StdOrder	RunOrder	PtType	Blocks	A	B	C	Resp
1	1	2	1	−1	−1	0	78.04
13	2	0	1	1	−1	0	81.1
2	3	2	1	−1	1	0	86.62
8	4	2	1	1	1	0	87.05
15	5	0	1	−1	0	−1	77.24
6	6	2	1	1	0	−1	83.25
9	7	2	1	−1	0	1	80.73
14	8	0	1	1	0	1	81.53
10	9	2	1	0	−1	−1	84.61
3	10	2	1	0	1	−1	87.95
7	11	2	1	0	−1	1	89.9
4	12	2	1	0	1	1	92.15
5	13	2	1	0	0	0	85.91
11	14	2	1	0	0	0	85.69
12	15	2	1	0	0	0	85.29

the radiolabeled nanoconjugate exhibited significant stability under these studied conditions. The low levels of transchelation in both environments suggested that the radiotracer maintained its integrity and remained suitable for potential use in further experiments and applications.

3.5. Scintigraphy and biodistribution studies

To assess the accumulation of ^{99m}Tc-GQDs–pembrolizumab in tumor tissues, SPECT scans were conducted on mice bearing 4T1 tumors, one hour following the intravenous injection of 7.4 MBq of the radiotracer

Table 3
Results of variance analysis.

Term	Coef	SE Coef	T-Value	P-Value
Constant	85.63	1.13	76.05	0.000
A	1.287	0.689	1.87	0.121
B	2.515	0.689	3.65	0.015
C	1.408	0.689	2.04	0.097
A*A	−5.20	1.01	−5.12	0.004
B*B	2.77	1.01	2.73	0.041
C*C	0.25	1.01	0.25	0.813
A*B	−0.657	0.975	−0.67	0.530
A*C	−1.303	0.975	−1.34	0.239
B*C	−0.273	0.975	−0.28	0.791

(as shown in Fig. 9). The SPECT images clearly demonstrated a high level of uptake of ^{99m}Tc-GQDs–pembrolizumab (8.4 %ID/g) in the tumor area. In addition, SPECT scans were also performed on normal mice injected with ^{99m}Tc-GQDs–pembrolizumab, revealing significant accumulation of the radiotracer in the liver. The biodistribution profile of ^{99m}Tc-GQDs–pembrolizumab, acquired two hours post-injection into the tail vein of 4T1 tumor-bearing mice, was presented in Fig. 10. These results provided valuable insight into the distribution and accumulation of the radiotracer in various tissue and organs, emphasizing the potential of the developed nanoparticle-antibody conjugate for targeted imaging applications.

4. Discussion

The introduction of a relatively novel approach involving the conjugation of antibodies with nanoparticles has opened up significant opportunities across various domains, with particular emphasis on the advancement of tumor imaging platforms (Lin et al., 2021, Shanehsazzadeh et al., 2015, Chen et al., 2020). These platforms offer a range of attractive properties, such as enhanced therapeutic effects within targeted tissues, improved cellular uptake, reduced side effects, and heightened specificity and sensitivity in diagnostic assessments (Juan et al., 2020). Numerous studies have been conducted to validate the potential of nanoparticles decorated with antibodies as effective agents for nuclear imaging (Wong et al., 2020, Wu et al., 2019). This innovative approach holds promise for advancing both therapeutic and diagnostic applications in the field of oncology and beyond. Certainly, the study conducted by Chen et al. presented a noteworthy example of utilizing ultrasmall silica nanoparticles that were conjugated with anti-human epidermal growth factor receptor 2 (HER2) single-chain variable fragments. These nanoparticles were further radiolabeled with ^{89}Zr to facilitate in vivo HER2-targeted PET imaging. The results of their investigation indicated promisingly high uptake levels in xenograft breast cancer models exhibiting HER2 +. Moreover, the study highlighted the nanoparticles' efficient renal clearance, which is a desirable characteristic for potential clinical applications (Chen et al., 2020). The combined approach of nanoparticle conjugation and radiolabeling with a targeting ligand holds significant potential for enhancing the accuracy and specificity of cancer imaging techniques, particularly in cases where specific biomarkers like HER2 are involved. The Recent development of N-doped graphene quantum dot (GQDs) and their subsequent radiolabeling with ^{99m}Tc represented a significant advancement in the field of molecular imaging. The optimization of the radiolabeling process to achieve a high radiochemical purity (RCP) of over 95 % underscores the importance of fine-tuning various parameters to ensure the successful preparation of the radiotracer. In this context, investigating parameters that affect the radiolabeling process, such as the concentrations of the nanoprobe (N-doped GQDs), reducing agent, ascorbic acid (antioxidant agent), pH, and temperature during the radiolabeling reaction, is critical. These factors can influence the efficiency of the radiolabeling process, the stability of the resulting radiotracer, and its targeting specificity. The use of N-doped GQDs as a platform for radiolabeling offers several advantages, including their tunable surface chemistry, biocompatibility, and potential for active targeting. The optimization of

Table 4
Calculated number of variables for optimal radiolabeling.

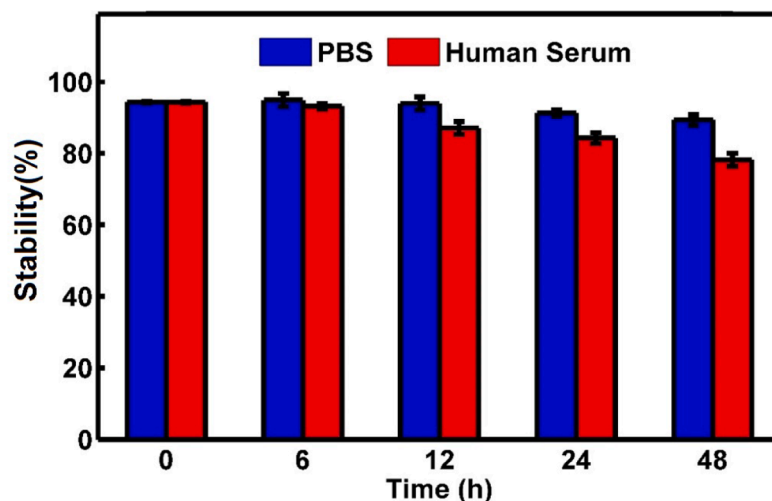| Time (min)	Reduced agent (mg)	GQDs–pembrolizumab (mg)	Resp$_{max}$
25	5	20	95.37
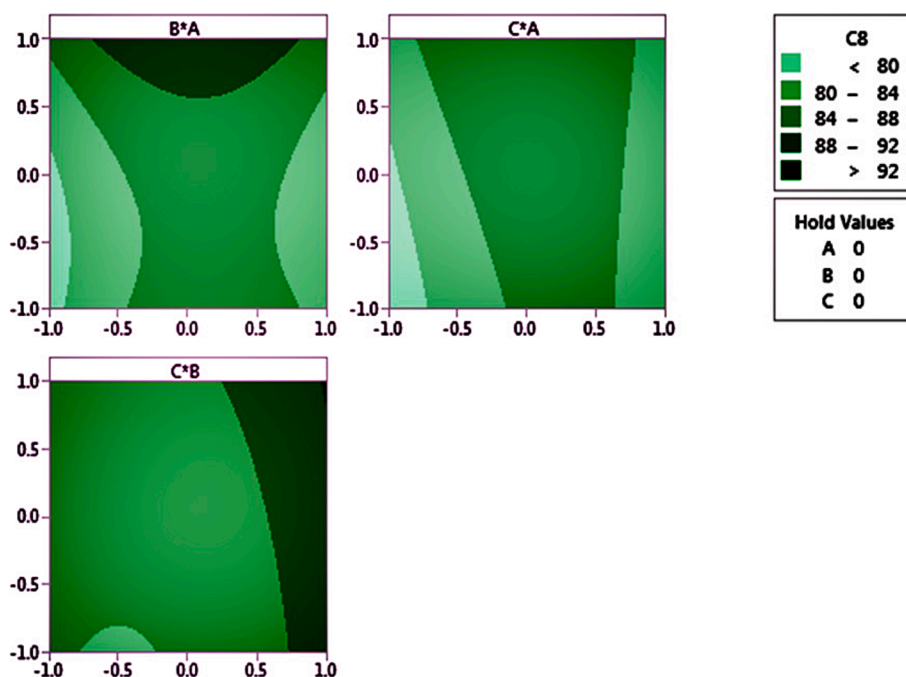
Fig. 7. Three sets of 2D images showing the interaction between the reducing agent and nanoconjugate (above-left), the interaction between the reducing agent and the time it takes (above-Right), and the interaction between time and the nanoconjugate (bottom).

a)
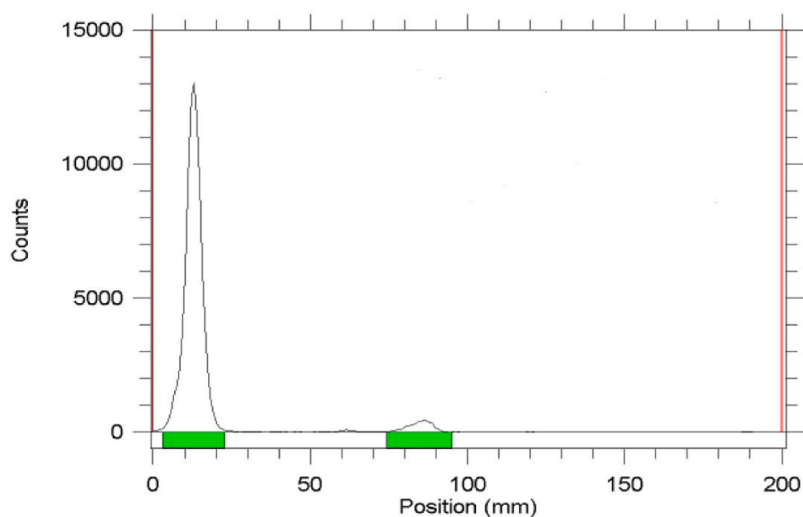
b)

Fig. 8. A) radio-chromatogram of free[99m]Tc and ^{99m}Tc-GQDs–pembrolizumab. b) In vitro stability of ^{99m}Tc-GQDs–pembrolizumab in PBS at 4 °C (blue) and in human serum at 37 °C (red) at various time intervals. (For interpretation of the references to color in this figure legend, the reader is referred to the web version of this article.)

the radiolabeling process ensure that the radiotracer can be synthesized reproducibly and reliably, meeting the quality and safety standards required for preclinical and clinical imaging studies. The imaging and biodistribution studies conducted on healthy Wistar rats have provided valuable insights into the behavior of the radiolabeled N-doped GQDs (^{99m}Tc-N-GQDs) in vivo (Gharepapagh et al., 2021).

Pembrolizumab, a humanized IgG$_4$ monoclonal antibody, has shown remarkable antitumor activity and a favorable safety profile in various clinical settings. One of its key mechanisms of action is its ability to inhibit the interaction between PD-1 and its ligands, PD-L1 and PD-L2. Recently, this approved anti-PD-1 antibody has been successfully radiolabeled with [89]Zr to investigate in vivo biological behavior and pharmacokinetics. Whole-body PET imaging and distribution studies in humanized mice demonstrated a high uptake of [89]Zr-pembrolizumab in

the lymph nodes, spleen and, bone marrow, indicating affinity for lymphoid tissues.[20] In 2022, two papers were published that involved the radiolabeling of pembrolizumab with ([89]Zr) and evaluated its clinical response through PD-1/PD-L1 blocking PET imaging. Twelve patients with non-small cell lung cancer (NSCLC) were chosen for PET/CT scans following injection of [89]Zr-pembrolizumab. The obtained results indicated a safe profile, and the radiotracer exhibited high uptake in the tumor lesions, liver, spleen, and the blood pool (Niemeijer et al., 2022). In another study, a cohort of 11 melanoma patients and 7 NSCLC patients underwent whole-body PET imaging to evaluate PD-1 expression and pembrolizumab biodistribution (Kok et al., 2022). The radiotracer exhibited notable accumulation in lymphoid tissues and sites of inflammation.

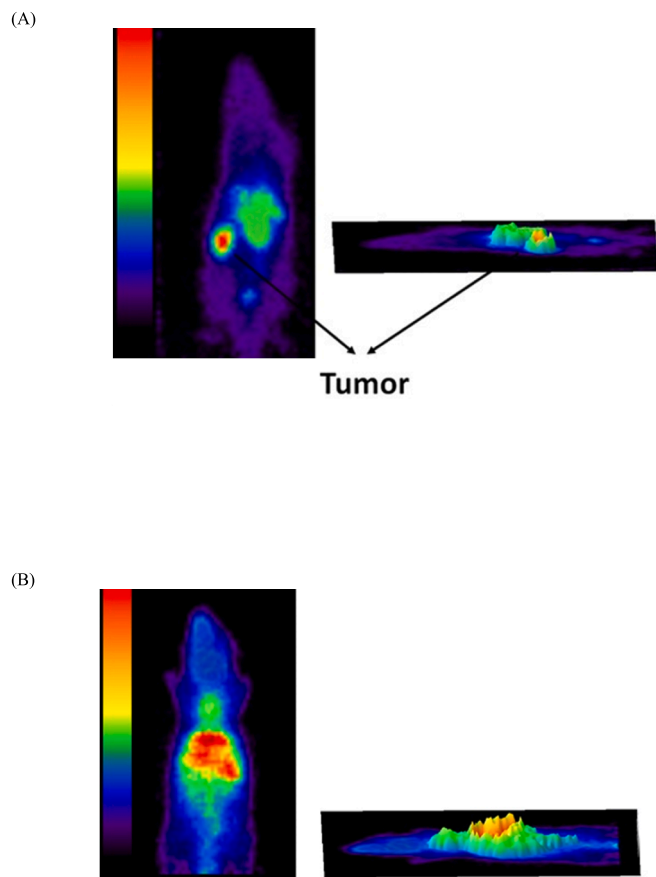This study marks a pioneering achievement as it encompasses the

(A)

(B)

Fig. 9. SPECT imaging performed one hour after the injection of 7.4 MBq of ^{99m}Tc-GQDs–pembrolizumab into the tail vein of BALB/c mice bearing 4 T1 tumors (A) and normal mice (B).

synthesis of GQDs, their successful conjugation with pembrolizumab, and the subsequent radiolabeling with ^{99m}Tc for the purpose of SPECT imaging in 4T1 tumor-bearing BALB/c mice. GQDs were synthesized in an aqueous solution utilizing a one-pot hydrothermal process involving urea and citric acid. Subsequently, successful conjugation of these nanoparticles with pembrolizumab was achieved. To comprehensively characterize both GQDs and GQDs–pembrolizumab conjugate, a range of analytical techniques were employed. These included TEM, AFM, Element Mapping, FT-IR, and CD spectroscopy. The GQDs exhibited favorable morphological and topographical characteristics. According to the TEM analysis, the particle size was determined to have an average diameter of 4.22 ± 1.5 nm. The FT-IR and CD spectra provided confirmatory evidence of successful conjugation between the nanoparticles and antibodies. These observations collectively underscored the effective integration of GQDs with pembrolizumab. The presence of the peak at 1654 cm^{-1} indicated the occurrence of amide bonding within the structure of the nanoconjugate. CD spectroscopy is a valuable technique for probing protein interactions with other molecules. Thus, the secondary structure of both pembrolizumab and the nanoconjugate was assessed using the far ultraviolent region (190–250 nm). The CD spectra of pembrolizumab and the nanoconjugate exhibited comparable patterns, signifying that the nanoconjugate maintained its proper folding. Furthermore, 2D and 3D AFM images of the GQDs-pembrolizumab conjugate revealed the morphological changes accompanied by an increase in size. The elemental mapping data obtained from scanning electron microscopy supported the presence of nitrogen, carbon, oxygen, and sulfur as the primary constituents of the nanoconjugate. Furthermore, the chelator-to-antibody ratio was computed and found to be 1.48 for the conjugation process.

Based on the statistical analysis of the data obtained from the MTT assay, both pembrolizumab and the synthesized GQDs-pembrolizumab conjugate exhibited no significant toxicity on the HEK-293 cells, which served as normal cells, at any concentration after 48 h of exposure. However, the anticancer activity of pembrolizumab and the nanoconjugate against the 4T1 murine breast cancer cell line had significantly reduced the cell viability percentage at the studied concentrations. The nanoconjugate demonstrated a substantial anticancer effect on the 4T1 cells than pembrolizumab lonely. Since the 4T1 cell line expressed the PD-1 receptor on its surface, in contrast to the HEK-293 cell line, these results might be associated with this difference.

Moreover, real-time binding analysis was conducted at 25 °C utilizing an SPR biosensor, specifically the Biacore 8 K system (GE Healthcare). The dissociation constant (KD) was determined to be approximately 0. 75 nM.

For radiolabeling of nanoparticles, a chelator-free procedure offers a convenient alternative to chelator-mediated methods. This approach eliminates the need for a multi-step chelator conjugation process, while preserving the inherent properties of the nanoparticles such as surface charge, size, and in vivo biodistribution and pharmacokinetics. Moreover, the direct labeling of nanoparticles with radiometals through simple, time-saving, and cost-effective surface interactions facilitates the translation of preclinical studies into clinical applications (Shi et al., 2017, Karpov et al., 2022, Tang et al., 2019). In this context, it is worth mentioning a recently developed biofriendly pentamodal imaging agent with synergistic dual-targeting abilities (both passive and active). This agent was based on fluoromagnetic NaGdF$_4$:Yb,Er upconverting nanoparticles (UCNPs). Apart from nano-enabled passive targeting, the conjugation with apo-human serum transferrin protein (Tf) actively targeted the transferrin receptors (TfR) overexpressed on various cancer cells. The noteworthy aspect of this agent was its chelator-free radiolabeling with ^{99m}Tc, indicating a radiolabeling efficiency approximately more than 95 % and stability of around 100 % for 24 h. Furthermore, it's in vitro stability exceeding 90 % over 24 h under various conditions was considered ideal for in vivo applications (Akhtar et al., 2022).

Therefore, in the study, we achieved favorable radiolabeling properties for ^{99m}Tc-GQDs–pembrolizumab through the use of a chelator-based approach eliminating the complications associated with the usual chelator conjugation process. These properties included high RCP (>95 %) and good in vitro stability in both PBS at 4 °C and human serum at 37 °C. The COOH groups on the surface of GQDs, as well as within the structure of pembrolizumab, act as hosts for the chelation of ^{99m}Tc. In Fig. 8a, the radio-chromatogram of the mobile free ^{99m}Tc moved approximately 85 mm compared to the ^{99m}Tc-GQDs–pembrolizumab, which stayed at the bottom around the 13 mm position on the TLC paper. The radiolabeling efficiency of ^{99m}Tc-GQDs–pembrolizumab was determined to be >95 %, demonstrating a comparable RCP to previously reported cases where pembrolizumab was conjugated with the tetrafluorphenol-N-succinyldesferal-Fe(III) ester (TFP-N-sucDf) as a chelator and radiolabeled with ^{89}Zr (van der Veen et al., 2020).

SPECT/CT whole-body imaging studies were conducted on both normal and 4T1 tumor-bearing BALB/c mice after intravenous administration of ^{99m}Tc-GQDs–pembrolizumab. The imaging results revealed notable accumulation of the radiotracer in tumor cells, as well as in healthy tissues such as the liver and spleen. Similarly, in the normal mice, there was significant uptake of ^{99m}Tc-GQDs–pembrolizumab observed in the liver and spleen. The PD-1 cell surface protein is primarily expressed on activated T and B lymphocytes (T and B cells), which are present at low levels in the 4T1 tumor-bearing mice. The principal organs that play a central role in the immune system response include the spleen, lymph nodes, and bone marrow. Based on the biodistribution results, increased radiotracer activity was observed in the liver, spleen, and tumor of BALB/c mice. Additionally, the biodistribution profiles of ^{99m}Tc-GQDs–pembrolizumab in both normal mice and 4T1 tumor-bearing BALB/c mice exhibited similarity. This study effectively demonstrated the strategic distribution of ^{99m}Tc-

(a)
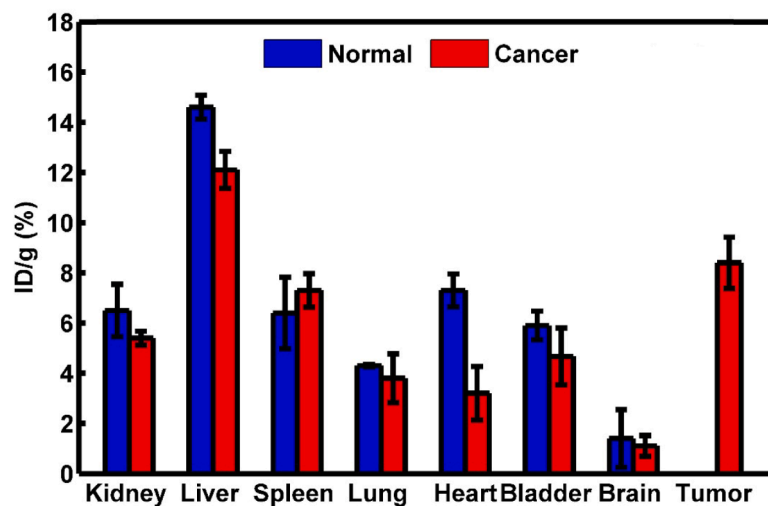
(b)
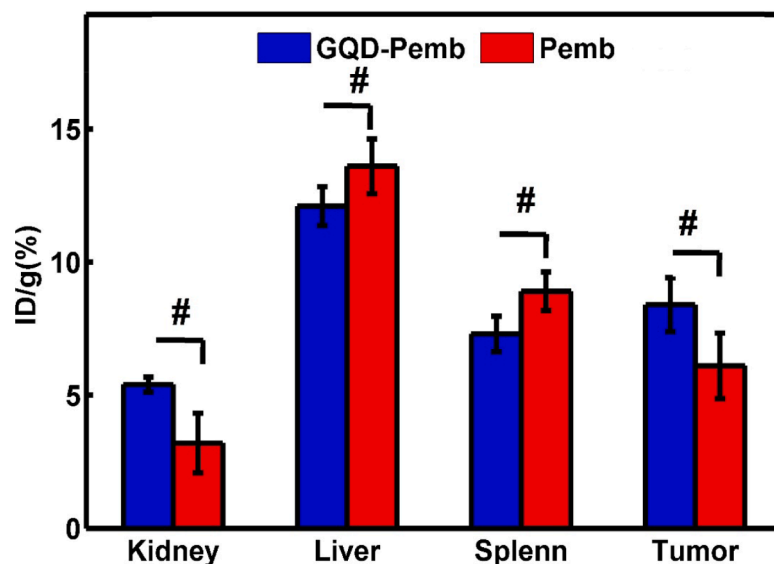
Fig. 10. Ex vivo biodistribution profile of a) ^{99m}Tc-GQDs–pembrolizumab two hours after injection into tail vein of normal mice and mice bearing 4 T1 tumors (a), and b) ^{99m}Tc-GQDs–pembrolizumab and ^{99m}T–pembrolizumab two hours after injection into tail vein of mice bearing 4 T1 tumors with the measurement given in "dose per gram of tissue.", It also indicates that "P-value < 0.05" was observed, signifying significance among different tissues.

GQDs–pembrolizumab to lymphoid organs with a high expression of PD-1 receptors. High uptake (8.4 %ID/g) of the radiotracer in tumor cells could potentially correlate with immunotherapy response, while uptake in lymphoid organs might relate to potential toxic effects. The activity detected in the kidney and bladder reflected the relative excretion of ^{99m}Tc-GQDs–pembrolizumab through the renal clearance system. Moreover, the tumor-to-muscle (T/M) ratios for ^{99m}Tc-GQDs–pembrolizumab was 0.73 ± 0.21 (P > 0.05).

Furthermore, to show the important role of GQDs, the ex vivo biodistribution data of ^{99m}Tc-GQDs–pembrolizumab and ^{99m}Tc- pembrolizumab two hours after injection (dose per gram of tissue) were conducted and are exhibited in Fig. 10. According to these data, uptake of ^{99m}Tc-GQDs–pembrolizumab and ^{99m}Tc-pembrolizumab in the tumor were 8.4 %ID/g and 6.1 %ID/g, respectively. In addition, uptake of ^{99m}Tc-GQDs–pembrolizumab and ^{99m}Tc- pembrolizumab in the kidney were 5.4 %ID/g and 3.2 %ID/g, respectively. Accumulation in the liver and spleen were 12.1 %ID/g and 7.3 %ID/g for ^{99m}Tc-GQDs–pembrolizumab and 13.6 %ID/g and 8.9 %ID/g for ^{99m}Tc-pembrolizumab. In fact, using GQDs led to higher uptake of the radiotracer in the tumor and facilitated renal clearance to a greater extent. Our biodistribution assessment results demonstrated a significantly higher tumor uptake compared to the liver and spleen, in contrast to the results of ^{89}Zr-pemprolizumab (van der Veen et al., 2020). It appears that our nano-construct enables more efficient renal clearance, making it more convenient for nuclear medicine applications. This capability holds the potential to markedly improve the signal-to-background ratio, facilitating more precise diagnoses, and concurrently lowering the risk of toxicity, thereby enhancing the overall efficacy of treatments.
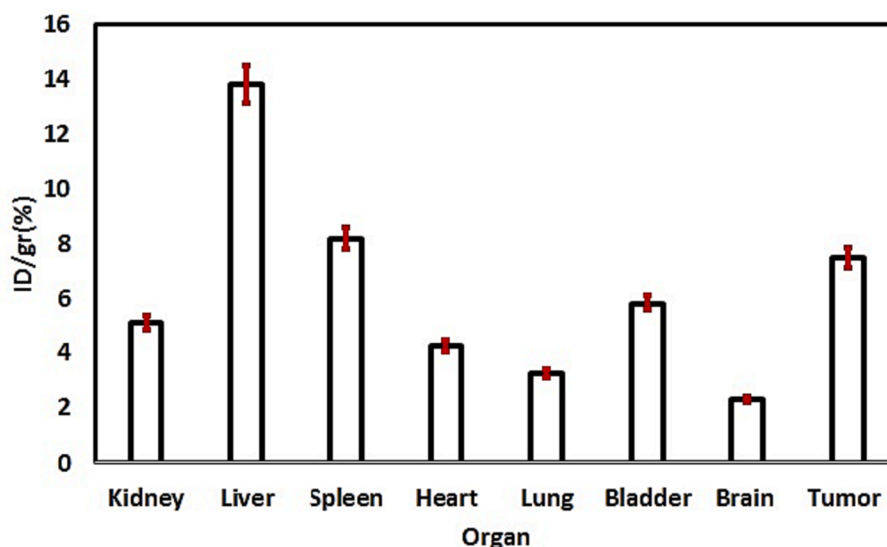
Fig. 11. Biodistribution profile of ^{99m}Tc-GQDs–pembrolizumab two hours after injection into tail vein of nude mice bearing human breast cancer (MDA-MB-231) cell line (P-value < 0.05).

Additionally, we performed biodistribution studies utilizing human breast cancer (MDA-MB-231) cell line and xenografted nude mice, reporting the results and comparing them to the previous reported findings, which exhibited similarity. This indicates the effective functionality of the synthetic radiotracer in diagnosing tumors in both human and murine breast cancer cell line (Fig. 11).

The promising attributes of ^{99m}Tc-GQDs-pembrolizumab encompassed straightforward synthesis, safety, availability, and cost-effectiveness of ^{99m}Tc, high radiochemical purity through chelator-based labeling, suitable in vitro stability, robust imaging capabilities, and a favorable biodistribution profile. Nonetheless, further comprehensive investigations are warranted to thoroughly delineate the complete spectrum of properties of this radiotracer for its near-future clinical application.

5. Conclusion

The present study introduces a novel class of imaging probes utilizing GQDs, which were conjugated to pembrolizumab and subsequently radiolabeled with ^{99m}Tc using a straightforward and efficient approach. The investigation included SPECT imaging and in vivo biodistribution studies conducted on mouse models. Accumulation of the radiotracer in the tumor and immune-related organs such as liver and spleen, attributed to the presence of PD-1 receptor. A stable and biocompatible nanoformulation, ^{99m}Tc-GQDs-pembrolizumab, with active targeting, has been demonstrated. This radiotracer ensured much safer renal clearance, a crucial requirement for clinical applications. The development and synthesis of these contrast agents have the potential to advance our understanding of the in vivo behavior of immune checkpoint monoclonal antibodies, thereby providing valuable insights into the mechanisms and dynamics of immune checkpoint inhibition therapy.

Declaration of competing interest

The authors declare that they have no known competing financial interests or personal relationships that could have appeared to influence the work reported in this paper.

Acknowledgments

References

Akhtar, N., Wen, P., Chen, C.L., et al., 2022. Radiolabeled human protein-functionalized upconversion nanoparticles for multimodal cancer imaging. ACS Appl. Nano Mater. 5, 7051–7062. https://doi.org/10.1021/acsanm.2c01016.

Amin, K.C., Saha, G.B., Go, R.T., 1997. A rapid chromatographic method for quality control of technetium-99m-bicisate. J. Nucl. Med. Technol. 25, 49–51.

Arnold, M., Morgan, E., Rumgay, H., et al., 2022. Current and future burden of breast cancer: Global statistics for 2020 and 2040. Breast 66, 15–23. https://doi.org/10.1016/j.breast.2022.08.010.

Banerjee, S., Pillai, M.R., Ramamoorthy, N., 2001. Evolution of Tc-99m in diagnostic radiopharmaceuticals. Semin. Nucl. Med. 31, 260–277. https://doi.org/10.1053/snuc.2001.26205.

Boussiotis, V.A., 2016. Molecular and biochemical aspects of the PD-1 checkpoint pathway. N. Engl. J. Med. 375, 1767–1778. https://doi.org/10.1056/NEJMra1514296.

Brahmer, J., Reckamp, K.L., Baas, P., et al., 2015. Nivolumab versus docetaxel in advanced squamous-cell non-small-cell lung cancer. N. Engl. J. Med. 373, 123–135. https://doi.org/10.1056/NEJMoa1504627.

Broos, K., Lecocq, Q., Raes, G., et al., 2018. Noninvasive imaging of the PD-1:PD-L1 immune checkpoint: Embracing nuclear medicine for the benefit of personalized immunotherapy. Theranostics. 8, 3559–3570. https://doi.org/10.7150/thno.24762.

Carbognin, L., Pilotto, S., Milella, M., et al., 2015. Differential activity of nivolumab, pembrolizumab and MPDL3280A according to the tumor expression of Programmed Death-Ligand-1 (PD-L1): sensitivity analysis of trials in melanoma lung and genitourinary cancers. PLoS One 10, 0130142. https://doi.org/10.1371/journal.pone.0130142.

Cassette, E., Helle, M., Bezdetnya, L., et al., 2013. Design of new quantum dot materials for deep tissue infrared imaging. Adv. Drug Deliv. Rev. 65, 719–731. https://doi.org/10.1016/j.addr.2012.08.016.

Chen, J.S., Chen, J., Bhattacharjee, S., et al., 2020. Functionalized nanoparticles with targeted antibody to enhance imaging of breast cancer in vivo. J. Nanobiotechnol. 18, 135. https://doi.org/10.1186/s12951-020-00695-2.

Chinen, A.B., Guan, C.M., Ferrer, J.R., et al., 2015. Nanoparticle probes for the detection of cancer biomarkers, cells, and tissues by fluorescence. Chem. Rev. 115, 10530–10574. https://doi.org/10.1021/acs.chemrev.5b00321.

Decristoforo, C., Zolle, I., Rakias, F., et al., 2007. Quality Control Methods of 99mTc Pharmaceuticals. Technetium-99m Pharmaceuticals: Preparation and Quality Control in Nuclear Medicine. Berlin, Heidelberg: Springer Berlin Heidelberg, p. 123.

Ehlerding, E.B., England, C.G., McNeel, D.G., et al., 2016. Molecular imaging of immunotherapy targets in cancer. J. Nucl. Med. 57, 1487–1492. https://doi.org/10.2967/jnumed.116.177493.

England, C.G., Ehlerding, E.B., Hernandez, R., et al., 2017. Preclinical pharmacokinetics and biodistribution studies of 89Zr-labeled pembrolizumab. J. Nucl. Med. 58, 162–168. https://doi.org/10.2967/jnumed.116.177857.

Gharepapagh, E., Fakhari, A., Firuzyar, T., et al., 2021. Preparation, biodistribution and dosimetry study of Tc-99m labeled N-doped graphene quantum dot nanoparticles as

a multimodular radiolabeling agent. New J. Chem. 45, 3909–3919. https://doi.org/10.1039/D0NJ04762G.

Ghoreishi, S.M., Najdian, A., Yadegari, S., et al., 2020. The use of carbon quantum dot as alternative of stannous chloride application in radiopharmaceutical kits. Contrast Media Mol. Imaging 2020, 4742158. https://doi.org/10.1155/2020/4742158.

Gu, S., Hsieh, C., Yuan, C., et al., 2020. Fluorescence of functionalized graphene quantum dots prepared from infrared-assisted pyrolysis of citric acid and urea. J. Lumin. 217, 116774 https://doi.org/10.1016/j.jlumin.2019.116774.

Guo, B., Zuo, Y., Shi, Y., et al., 2020. Transmission electron microscopy-based statistical analysis of commercially available graphene oxide quantum dots. Cryst. Res. Technol. 55, 1900231. https://doi.org/10.1002/crat.201900231.

Hamid, O., Carvajal, R.D., 2013. Anti-programmed death-1 and anti-programmed death-ligand 1 antibodies in cancer therapy. Expert Opin. Biol. Ther. 13, 847–861. https://doi.org/10.1517/14712598.2013.770836.

Hassanpouraghdam, Y., Pooresmaeil, M., Namazi, H., 2022. In-vitro evaluation of the 5-fluorouracil loaded GQDs@Bio-MOF capped with starch biopolymer for improved colon-specific delivery. Int. J. Biol. Macromol. 221, 256–267. https://doi.org/10.1016/j.ijbiomac.2022.08.167.

Hsueh, E.C., Gorantla, K.C., 2015. Novel melanoma therapy. Exp. Hematol. Oncol. 5, 23. https://doi.org/10.1186/s40164-016-0054-1.

Inokuchi, J., Eto, M., 2019. Profile of pembrolizumab in the treatment of patients with unresectable or metastatic urothelial carcinoma. Cancer Manage. Res. 11 (4519–4528), 4528. https://doi.org/10.2147/CMAR.S167708.

Jia, X., Campos-Delgado, J., Terrones, M., et al., 2011. Graphene edges: a review of their fabrication and Characterization. Nanoscale 3, 86–95. https://doi.org/10.1039/C0NR00600A.

Juan, A., Cimas, F.J., Bravo, I., et al., 2020. Antibody conjugation of nanoparticles as therapeutics for breast cancer treatment. Int. J. Mol. Sci. 21, 6018. https://doi.org/10.3390/ijms21176018.

Kao, H.W., Lin, Y.Y., Chen, C.C., et al., 2014. Biological characterization of cetuximab-conjugated gold nanoparticles in a tumor animal model. Nanotechnology 25, 295102. https://doi.org/10.1088/0957-4484/25/29/295102.

Karpov, T., Postovalova, A., Akhmetova, D., et al., 2022. Universal chelator-free radiolabeling of organic and inorganic-based nanocarriers with diagnostic and therapeutic isotopes for internal radiotherapy. Chem. Mater. 34, 6593–6605. https://doi.org/10.1021/acs.chemmater.2c01507.

Kok, I.C., Hooiveld, J.S., van de Donk, P.P., et al., 2022. 89Zr-pembrolizumab imaging as a non- invasive approach to assess clinical response to PD-1 blockade in cancer. Ann. Oncol. 33, 80–88. https://doi.org/10.1016/j.annonc.2021.10.213.

Kono, Y., Utsunomiya, K., Kan, N., et al., 2021. A comparison of HER2/neu accumulations of Ga-67-labeled anti-HER2 antibody with chemically and site-specifically conjugated bifunctional chelators. Cancer Treat Res. Commun. 27, 100333 https://doi.org/10.1016/j.ctarc.2021.100333.

Kumar, Y.R., Deshmukh, K., Sadasivuni, K.K., et al., 2020. Graphene quantum dot based materials for sensing, bio-imaging and energy storage applications: a review. RSC Adv. 10, 23861–23898. https://doi.org/10.1039/D0RA03938A.

Kwok, G., Yau, T.C.C., Chiu, J.W., et al., 2016. Pembrolizumab (Keytruda). Hum. Vaccin. Immunother. 12, 2777–2789. https://doi.org/10.1080/21645515.2016.1199310.

Lee, J.Y., Lee, H.T., Shin, W., et al., 2016. Structural basis of checkpoint blockade by monoclonal antibodies in cancer immunotherapy. Nat. Commun. 7, 13354. https://doi.org/10.1038/ncomms13354.

Lee, C.K., Man, J., Lord, S., et al., 2017. Checkpoint inhibitors in metastatic EGFR-mutated non-small cell lung cancer-A meta-analysis. J. Thorac. Oncol. 12, 403–407. https://doi.org/10.1016/j.jtho.2016.10.007.

Lee, J.H., Park, G., Hong, G.H., et al., 2012. Design considerations for targeted optical contrast agents. Quant. Imaging Med. Surg. 2, 266–273. https://doi.org/10.3978/j.issn.2223-4292.2012.12.04.

Li, L., Wu, G., Yang, G., et al., 2013. Focusing on luminescent graphene quantum dots: current status and future perspectives. Nanoscale 5, 4015–4039. https://doi.org/10.1039/C3NR33849E.

Lijowski, M., Caruthers, S., Hu, G., et al., 2009. High sensitivity: high-resolution SPECT-CT/MR molecular imaging of angiogenesis in the Vx2 Model. Investig. Radiol. 44, 15–22. https://doi.org/10.1097/RLI.0b013e31818935eb.

Lin, X., O'Reilly Beringhs, A., Lu, X., 2021. Applications of nanoparticle-antibody conjugates in immunoassays and tumor imaging. AAPS J. 23, 43. https://doi.org/10.1208/s12248-021-00561-5.

Liu, S., Edwards, D.S., 1999. 99mTc-Labeled small peptides as diagnostic radiopharmaceuticals. Chem. Rev. 99, 2235–2268. https://doi.org/10.1021/cr980436l.

Mahmoudi, M., Lynch, I., Ejtehadi, M.R., et al., 2011. Protein-nanoparticle interactions: opportunities and challenges. Chem. Rev. 111, 5610–5637. https://doi.org/10.1021/cr100440g.

Marhelava, K., Pilch, Z., Bajor, M., et al., 2019. Targeting negative and positive immune checkpoints with monoclonal antibodies in therapy of cancer. Cancers (basel) 11, 1756. https://doi.org/10.3390/cancers11111756.

Meerloo, J.V., Kaspers, G.J.L., Cloos, J., 2011. Cell sensitivity assays: the MTT assay. Methods Mol. Biol. 731, 237–245. https://doi.org/10.1007/978-1-61779-080-5_20.

Mura, S., Nicolas, J., Couvreur, P., 2013. Couvreur, Stimuli-responsive nanocarriers for drug delivery. Nat. Mater. 12, 991–1003. https://doi.org/10.1038/nmat3776.

Najdian, A., Amanlou, M., Beiki, D., et al., 2022. Amino-modified-silica-coated gadolinium-copper nanoclusters, conjugated to AS1411 aptamer and radiolabeled with technetium-99 m as a novel multimodal imaging agent. Bioorg. Chem. 125, 105827 https://doi.org/10.1016/j.bioorg.2022.105827.

Natarajan, A., Patel, C.B., Habte, F., et al., 2018. Dosimetry prediction for clinical translation of (64)Cu-Pembrolizumab ImmunoPET Targeting Human PD-1 expression. Sci. Rep. 8, 633. https://doi.org/10.1038/s41598-017-19123-x.

Niemeijer, A.N., Oprea-Lager, D.E., Huisman, M.C., et al., 2022. Study of 89Zr-Pembrolizumab PET/CT in patients with advanced-stage non-small cell lung cancer. J. Nucl. Med. 63, 362–367. https://doi.org/10.2967/jnumed.121.261926.

Nikzad, S., Hashemi, B., Hassan, Z.M., et al., 2013. The Cell Survival of F10B16 Melanoma and 4T1 breast adenocarcinoma irradiated to gamma radiation using the MTT assay based on two different calculation methods. J. Biomed. Phys. Eng. 1 (3), 29–36.

Pan, J., Zhang, J., Li, Z., et al., 2010. Hydrothermal route for cutting graphene sheets into blue-luminescent graphene quantum dots. Adv. Mater. 22, 734–738. https://doi.org/10.1002/adma.200902825.

Passiglia, F., Bronte, G., Bazan, V., et al., 2016. PD-L1 expression as predictive biomarker in patients with NSCLC: a pooled analysis. Oncotarget 7, 19738–19747. https://doi.org/10.18632/oncotarget.7582.

Popovtzer, R., Agrawal, A., Kotov, N.A., et al., 2008. Targeted gold nanoparticles enable molecular CT imaging of cancer. Nano Lett. 8, 4593–4596. https://doi.org/10.1021/nl8029114.

Psimadas, D., Bouziotis, P., Georgoulias, P., et al., 2013. Radiolabeling approaches of nanoparticles with 99mTc. Contrast Media Mol. Imaging 8 (4), 333–339. https://doi.org/10.1002/cmmi.1530.

Rai, Y., Pathak, R., Kumari, N., et al., 2018. Mitochondrial biogenesis and metabolic hyperactivation limits the application of MTT assay in the estimation of radiation induced growth inhibition. Sci. Rep. 8, 1531. https://doi.org/10.1038/s41598-018-19930-w.

Ryu, J., Lee, E., Lee, S., et al., 2014. Fabrication of graphene quantum dot-decorated graphene sheets *via* chemical surface modification. Chem. Commun. 50, 15616–15618. https://doi.org/10.1039/C4CC06567K.

Saresella, M., Rainone, V., Al-Daghri, N.M., et al., 2012. The PD-1/PD-L1 pathway in human pathology. Curr. Mol. Med. 12, 259–267. https://doi.org/10.2174/156652412799218903.

Shanehsazzadeh, S., Gruettner, C., Lahooti, A., et al., 2015. Monoclonal antibody conjugated magnetic nanoparticles could target MUC-1-positive cells in vitro but not in vivo. Contrast Media Mol. Imaging 10, 225–236. https://doi.org/10.1002/cmmi.1627.

Shi, S., Xu, C., Yang, K., et al., 2017. Chelator-Free Radiolabeling of Nanographene: Breaking the Stereotype of Chelation. Angew. Chem. Int. Ed. Engl. 56, 2889–2892. https://doi.org/10.1002/anie.201610649.

Siegel, R.L., Miller, K.D., Wagle, N.S., et al., 2023. Cancer statistics. CA: A Cancer J Clin. 73, 17–48. https://doi.org/10.3322/caac.21763.

Simanek, M., Koranda, P., 2016. SPECT/CT imaging in breast cancer - current status and challenges. Biomed. Pap. Med. Fac. Univ. Palacky Olomouc Czech Repub. 160, 474–483. https://doi.org/10.5507/bp.2016.036.

Tang, T., Wei, Y., Yang, Q., et al., 2019. Rapid chelator-free radiolabeling of quantum dots for in vivo imaging. Nanoscale 11, 22248–22254. https://doi.org/10.1039/C9NR08508D.

van der Veen, E.L., Giesen, D., Pot-de Jong, L., et al., 2020. (89)Zr-pembrolizumab biodistribution is influenced by PD-1-mediated uptake in lymphoid organs. J. Immunother. Cancer 8, e000938.

Wang, H., Mu, Q., Wang, K., et al., 2019. Nitrogen and boron dual-doped graphene quantum dots for near-infrared second window imaging and photothermal therapy. Appl. Mater. Today 14, 108–117. https://doi.org/10.1016/j.apmt.2018.11.011.

Wang, Y., Wei, H., 2019. 131I-labeled PEG and folic acid co-functionalized graphene quantum dots for tumor-targeted imaging. J. Radio Anal. Nucl. Chem. 319, 1119–1125. https://doi.org/10.1007/s10967-019-06434-8.

Wang, J., Yuan, R., Song, W., et al., 2017. PD-1, PD-L1 (B7–H1) and tumor-site immune modulation therapy: the historical perspective. J. Hematol. Oncol. 10, 34. https://doi.org/10.1186/s13045-017-0403-5.

Wong, P., Li, L., Chea, J., et al., 2020. Antibody targeted PET imaging of 64Cu-DOTA-Anti-CEA PEGylated Lipid Nanodiscs in CEA positive tumors. Bioconjug. Chem. 31, 743–753. https://doi.org/10.1021/acs.bioconjchem.9b00854.

Wu, C.Y., Lin, J.J., Chang, W.Y., et al., 2019. Development of theranostic active-targeting boron- containing gold nanoparticles for boron neutron capture therapy (BNCT). Colloids Surf. B Biointerfaces 183, 110387. https://doi.org/10.1016/j.colsurfb.2019.110387.

Xu, R., Zhang, G., Mai, J., et al., 2016. An injectable nanoparticle generator enhances delivery of cancer therapeutics. Nat. Biotechnol. 34, 414–418. https://doi.org/10.1038/nbt.3506.

Zheng, X.T., Ananthanarayanan, A., et al., 2015. Glowing graphene quantum dots and carbon dots: properties, syntheses, and biological applications. Small 11, 1620–2136. https://doi.org/10.1002/smll.201402648.

Zhou, X., Zhang, Y., Wang, C., et al., 2012. Photo-Fenton reaction of graphene oxide: a new strategy to prepare graphene quantum dots for DNA cleavage. ACS Nano 6, 6592–6599. https://doi.org/10.1021/nn301629v.